Collisional dependence of Alfvén mode saturation in tokamaks

IOP Publishing Plasma Physics and Controlled Fusion
Plasma Phys. Control. Fusion **58** (2016) 125006 (8pp) doi:10.1088/0741-3335/58/12/125006

Collisional dependence of Alfvén mode saturation in tokamaks

Muni Zhou[1] **and Roscoe White**[2]

[1] Physics Department, Zhejiang University, Hangzhou, People's Republic of China
[2] Plasma Physics Laboratory, Princeton University, PO Box 451, Princeton, NJ 08543, USA

E-mail: rwhite@pppl.gov

Received 31 May 2016
Accepted for publication 29 June 2016
Published 26 October 2016

Abstract

Saturation of Alfvén modes driven unstable by a distribution of high energy particles as a function of collisionality is investigated with a guiding center code, using numerical eigenfunctions produced by linear theory and numerical high energy particle distributions. The most important resonance is found and it is shown that when the resonance domain is bounded, not allowing particles to collisionlessly escape, the saturation amplitude is given by the balance of the resonance mixing time with the time for nearby particles to collisionally diffuse across the resonance width. Saturation amplitudes are in agreement with theoretical predictions as long as the mode amplitude is not so large that it produces stochastic loss from the resonance domain.

Keywords: Alfvén modes, saturation, collisions, tokamaks

S Online supplementary data available from stacks.iop.org/PPCF/58/125006/mmedia

(Some figures may appear in colour only in the online journal)

1. Introduction

The effect of Alfvén modes on energetic particles in tokamaks is important in general, and could be of significance for ITER [1]. It has been demonstrated that high energy injected beam driven Alfvén modes can significantly modify the beam particle distribution, either through profile modification or induced loss [2–6]. Previous work concerning the induced loss of beam particles due to Alfvén modes has used experimental values for mode amplitudes. Work is needed to be able to correctly predict mode amplitudes in current devices and in ITER in order to understand the presently observed beam density reduction and predict expected fast ion transport due to Alfvén modes. Significant loss can greatly diminish plasma heating and thus compromise the ability to achieve a burning plasma. When a sufficient number of modes reach a critical amplitude, stochastic transport of beam ions takes place. Thus the effect of the modes on beam density is a sensitive function of the mode saturation amplitudes. Mode saturation is a function of collisionality, since collisions move particles in and out of resonances responsible for instabilities, and there are several previous theoretical studies of the dependence of mode saturation on particle collisionality [7–10]. These studies however make use of analytic particle distributions, usually a simple bump on tail distribution, and also employ nonlinear fluid equations and a simple model mode eigenfunction. In this work we examine the dependence of mode saturation amplitudes on particle collisionality for a particular discharge in NSTX [11], making use of the numerical high energy beam particle distribution, and the full mode structure as predicted by a stability code, including many poloidal harmonics.

Solving the drift kinetic equation in the presence of Alfvén modes driven unstable by a distribution of high energy particles and advancing the mode amplitudes and phases in time is done with the use of a δf formalism, whereby the initial distribution f_0 is assumed to be a steady state high energy particle distribution in the absense of the modes, and $f = f_0 + \delta f$ describes the particle distribution in the presence of the modes. The Hamiltonian is written as $H = H_0 + H_1$ with H_0 giving the unperturbed motion, conserving particle energy E, toroidal canonical momentum P_ζ, and magnetic moment μ. The δf formalism and the construction of the initial high energy particle distribution are described in detail in another publication [12]. It is important to ascertain whether the scaling predictions

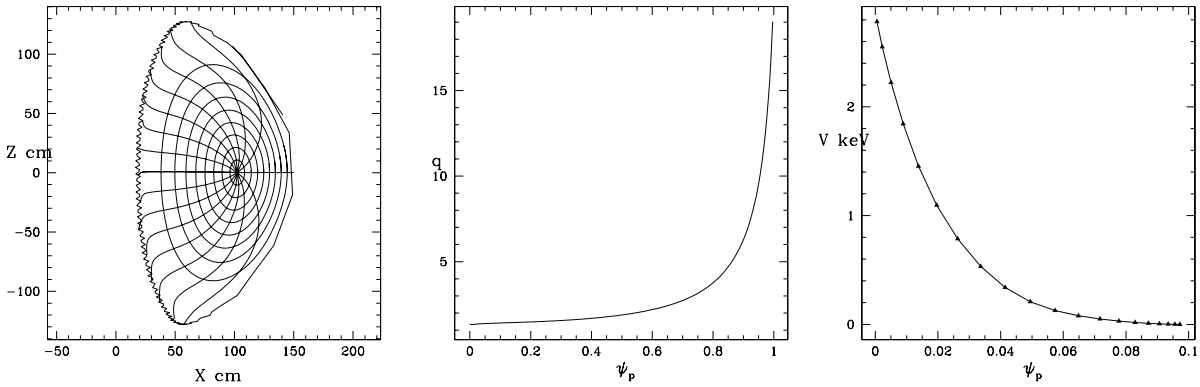

Figure 1. Equilibrium, showing the poloidal cross section with X and Z in centimeters (left), the q profile (center), and radial potential (right) for NSTX discharge 141711.

arising from idealized models is reproduced with a particle code using a δf formalism, actual mode eigenfunctions, and representations of the full equilibrium particle distribution.

In figure 1 is shown the NSTX equilibrium used, the q profile, and the potential associated with toroidal rotation. Plasma rotation, by modifying local toroidal velocities, can change the existence and location of mode-particle resonances.

In section 2 we briefly present the guiding center formalism, the representation of the mode used along with equations for advancing the modes in time, and the δf formalism used to find mode growth. In section 3 we give the numerical results. In section 4 we present a rapid means of determining single mode saturation amplitudes and a comparison with theoretical expressions. In section 5 are the conclusions.

2. Guiding center equations

We use units of time given by ω_0^{-1}, where $\omega_0 = eB/(mc)$ is the on-axis gyro frequency, B the magnetic field strength, e the charge and m the particle mass, and units of distance given by the major radius R. The basic unit of energy becomes $m\omega_0^2R^2$, which can also be written as $(mv^2/2)(2R^2/\rho^2)$, the gyro radius is $\rho = v/B \ll 1$, and the magnetic moment $\mu = v_\perp^2/(2B)$ is of order ρ^2 [13].

Kinetic Poincaré plots, made following high energy particle orbits in the presence of a perturbation with a single toroidal mode number and frequency, and recording points whenever $n\zeta - \omega t = 2\pi k$ with k integer, indicate mode-particle resonances and the island structure of these resonances. Location of mode-particle resonances is also a very delicate process requiring high accuracy [14–16]. The time scales of interest in mode saturation are given by the linear growth rate, the collision rate, the diffusion rate of particles in the vicinity of the resonance, and the resonance bounce frequency, giving the mixing time for particles trapped within a resonance. Because of the dependence of bounce time within a resonance on the distance from the resonance O-point, after a few bounce times the distribution within the resonance is irreversibly flattened, giving a final mixed state of higher entropy. This mixing time is thus a distribution averaged bounce time for particles within the resonance, giving the time scale for the flattening of the distribution at the resonance.

The duration of resonance and the replenishment of that part of the distribution within resonance is modified by particle collisions. Pitch angle scattering collisions, due to collisions with the background ions, are given by a simple energy conserving operator [17].

The equilibrium magnetic field is given by

$$\vec{B} = g\nabla\zeta + I\nabla\theta + \delta\nabla\psi_p, \tag{1}$$

with ψ_p the poloidal flux, ζ a toroidal angle coordinate, and θ a poloidal angle coordinate. The equilibrium is axisymmetric, thus independent of ζ. In an axisymmetric equilibrium using Boozer coordinates g and I are functions of ψ_p only. The Hamiltonian is

$$H_0 = \frac{\rho_\parallel^2 B^2}{2} + \mu B + \Phi \tag{2}$$

with $\rho_\parallel = v_\parallel/B$, μ the magnetic moment and Φ the electric potential [13]. Guiding center equations advance the variables ψ_p, θ, ζ, and $\rho_\parallel$, leaving μ a constant of the motion. The toroidal canonical momentum is

$$P_\zeta = g(\psi_p)\rho_\parallel - \psi_p. \tag{3}$$

The perturbation has the form $\delta\vec{B} = \nabla\times\alpha\vec{B}$ with

$$\alpha = \sum_{m,n} A_n\alpha_{m,n}(\psi)\sin(\Omega_{mn}), \Phi = \sum_{m,n} A_n\Phi_{m,n}(\psi)\sin(\Omega_{mn}), \tag{4}$$

where each mode has a given value of n and frequency, but many poloidal harmonics m, $\Omega_{mn} = n\zeta - m\theta - \omega_n t - \phi_n$, where ϕ_n is the mode phase, and for ideal modes the electric potential Φ is chosen to cancel the parallel electric field induced by $\mathrm{d}\vec{B}/\mathrm{d}t$, requiring

$$\sum_{m,n}\omega B\alpha_{m,n}\cos(\Omega_{mn}) - \vec{B}\cdot\nabla\Phi/B = 0.$$

and in Boozer coordinates

$$(gq + I)\omega\alpha_{mn} = (nq - m)\Phi_{mn}.$$

The perturbation α is related to the ideal displacement $\vec{\xi}$,

$$\alpha_{mn} = \frac{(m/q - n)}{(mg + nI)}\xi^\psi_{mn}.$$

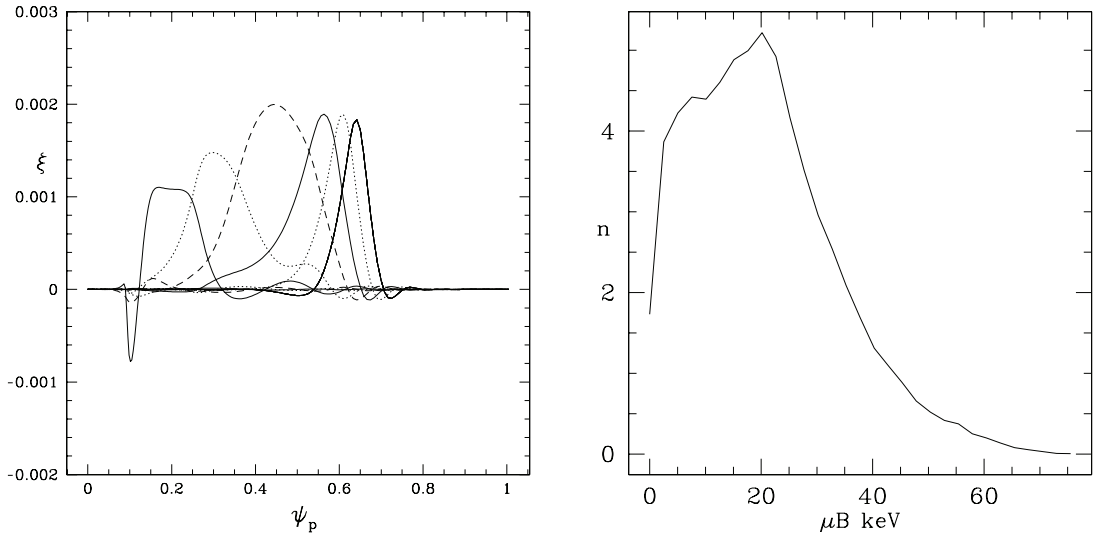

Figure 2. Harmonics of the 111 kHz, $n = 5$ mode with $5 \leqslant m \leqslant 13$ (left). Modes with $m < 8$ are too small to be seen, and the peaks, from left to right, correspond to modes with $m = 8,9,10,11,12,13$, in that order. The beam particle distribution in μ, (right) with particle density in arbitrary units, is seen to be strongly peaked at $\mu B = 20$ keV.

The numerically produced eigenfunctions are normalized with the largest harmonic $\xi^{\psi}_{mn}(\psi_{\rm p})$ having maximum amplitude 1. Thus the amplitude A_n is the magnitude of the ideal displacement caused by this harmonic, normalized to the major radius R, which is 100 cm, as seen in figure 1.

Stepping equations [18] for modes, with j the particle index are given by

$$\frac{{\rm d}A_n}{{\rm d}t} = \frac{-\nu_{\rm A}^2}{D_n\omega_n A_n}\sum_{j,m} w_n\Big[\rho_{\|}B^2\alpha_{mn}(\psi_{\rm p}) - \Phi_{mn}(\psi_p)\Big]\cos(\Omega_{mn}) - \gamma_{\rm d}A_n, \tag{5}$$

$$\frac{{\rm d}\phi_n}{{\rm d}t} = \frac{-\nu_{\rm A}^2}{D_n\omega_n A_n^2}\sum_{j,m} w_n\left[\rho_{\|}B^2\alpha_{mn}(\psi_{\rm p}) - \Phi_{mn}(\psi_{\rm p})\right]\sin(\Omega_{mn}), \tag{6}$$

with $D_n = 4\pi^2\sum_{\rm m}\int\xi^2_{mn}(\psi_{\rm p}){\rm d}\psi_{\rm p}$. $\gamma_{\rm d}$ is a linear damping rate including damping due to the continuum, radiation, thermal ion Landau damping, and electron Landau damping, and all terms in the sums are evaluated at the coordinates of particle j. The frequency $\nu_{\rm A}$ is the local Alfvén frequency and w_n is the weight of particle j for mode n. Collisions alter the mode evolution through the modification of the particle distribution, which of course modifies the values of equations (5) and (6). Mode saturation occurs when the distribution has been suficiently flattened in the vicinity of the resonances that the effective mode drive, including the damping and the effect of collisions, is reduced to zero.

The steady state distribution f_0 is a function only of the particle energy E, the canonical momentum P_ζ, and the magnetic moment μ. Since the mode frequencies under consideration are much below the cyclotron frequency, the modes do not change μ. The particle weights, which record the effect of the modes on the distribution, are stepped according to

$$\frac{{\rm d}w}{{\rm d}t} = \frac{w-1}{h(\psi_{\rm p},\theta,\zeta,\rho_{\|},0)}[\dot{E}\partial_E f_0 + \dot{P}_\zeta\partial_{P_\zeta}f_0]. \tag{7}$$

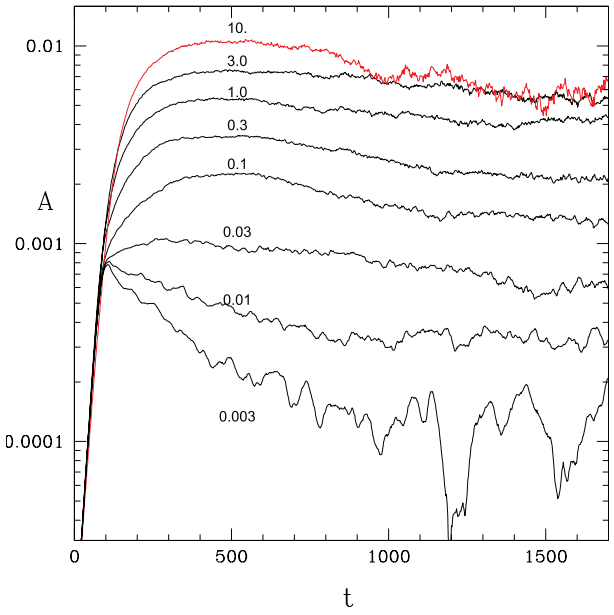

Figure 3. Time evolution of 111 kHz $n = 5$ TAE mode with collisionality of 0.003, 0.01, 0.03, 0.1, 0.3, 1, 3, 10 times the NSTX value of ν_0 . Shown is the amplitude of the largest harmonic in units of the major radius R, versus time.

with $h(\psi_{\rm p},\theta,\zeta,\rho_{\|},t)$ the distribution of marker particles, and the exchange of energy and momentum between the particle distribution and the modes is given by

$$\frac{{\rm d}E}{{\rm d}t} = \partial_t H = -\rho_{\|}B^2\partial_t\alpha + \partial_t\Phi,$$
$$\frac{{\rm d}P_\zeta}{{\rm d}t} = -\partial_\zeta H = \rho_{\|}B^2\partial_\zeta\alpha - \partial_\zeta\Phi. \tag{8}$$

The full particle distribution is given by $f = f_0 + \delta f$ and

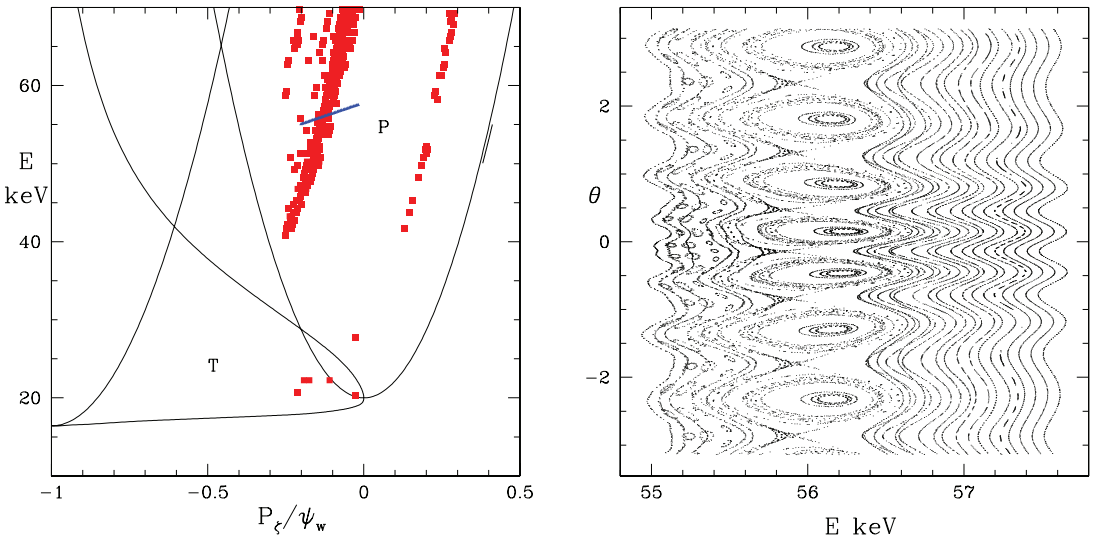

Figure 4. Plot of the P_ζ E plane showing the domain of broken KAM surfaces in red, and the line along which the Poincaré plot is made in blue (left), and the Poincaré plot (right). The mode amplitude was $A = 6 \times 10^{-4}$ for a 111 kHz $n = 5$ TAE mode. The plots are made for $\mu B = 20$ keV, where the distribution is strongly peaked, as seen in figure 2. The domains of passing and trapped particles have been labeled with P and T respectively.

$$\delta f(\psi_p, \theta, \zeta, \rho_\parallel, t) = \sum_j w\delta(\psi_p - \psi_{p,j}(t))\delta(\theta - \theta_j(t)) \times \delta(\zeta - \zeta_j(t))\delta(\rho_\parallel - \rho_{\parallel,j}(t)) \quad (9)$$

with the summation over j, the particle index. More detail concerning the δf formalism is given in [12].

3. Numerical results

We examine an unstable TAE mode in NSTX shot 141711 at 470 ms, with $n = 5$ and a frequency of 111 kHz. In distinction to previous simulations [7–9, 19–21], this work makes use of a numerical fit to the high energy beam distribution as given by TRANSP [22] rather than an analytic approximation. Details of the method for constructing the representation of the high energy beam distribution f_0 are given in reference [12]. The mode radial structure for the eigenvalues was supplied by NOVA [23, 24].

The radial structure of the poloidal harmonics of this 111 kHz, $n = 5$ mode are shown in figure 2. Poloidal mode numbers range from $m = 8$ to $m = 13$. Also shown is the beam particle distribution in the variable μB, in keV. The distribution is fairly strongly peaked at $\mu B = 20$ keV, as seen in figure 2, and we will use this value to examine the resonances. The obtained time evolution is shown for several different values of collisionality in figure 3 using 200 000 marker particles. A convenient unit of time for particle motion is the time for one toroidal transit of a particle on the magnetic axis with pitch 1 and a characteristic energy. The mode initially overshoots the final saturation amplitude, obtained in a little over 1000 toroidal transit times, or 3.3 ms. Initially the mode grows with $\gamma/\omega = 0.028$, and the damping, supplied by NOVA, was $\gamma_d/\omega = 0.0014$. The linear growth rate observed numerically

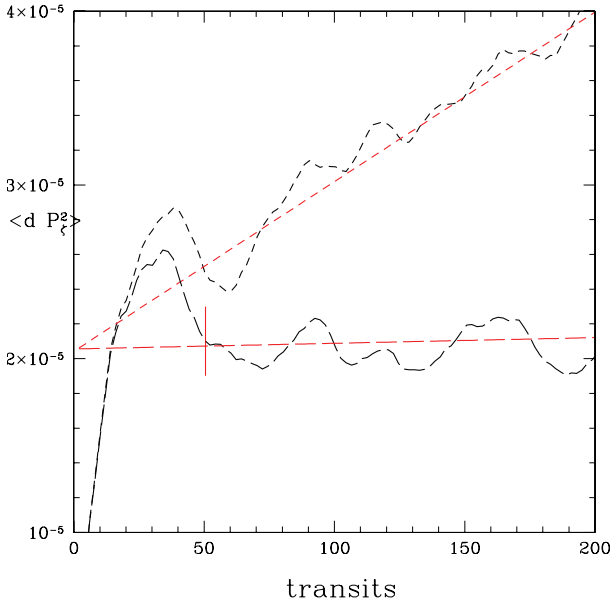

Figure 5. Local determination of $\langle dP_\zeta^2 \rangle$ versus time, in units of toroidal transits, with and without collisions. The plot approaching a constant in time is collisionless (long dashes), and that becoming linear in time is collisional (short dashes). In the collisionless case the width of the domain of broken KAM surfaces is given by the constant asymptotic value $W^2 = 2 \times 10^{-5}$ and in the collisional case the collisional diffusion rate is given by the asymptotic slope, a rate of $D = 9.8 \times 10^{-8}$. Shown in red are linear least square fits to the data, and with a solid vertical red line, the time taken as the mixing time, at $t = 50$. The parameters for the simulation were $E = 40$ keV, $\mu B = 20$ keV, and $P_\zeta/\psi_w = -0.27$, with amplitude $A = 3 \times 10^{-4}$ and collision rate $\nu = 0.003\,\nu_0$.

is larger than that predicted by NOVA, given as $\gamma/\omega = 0.017$. Thus this damping rate is much smaller than the linear growth rate, and has little if any effect on the simulation results. The

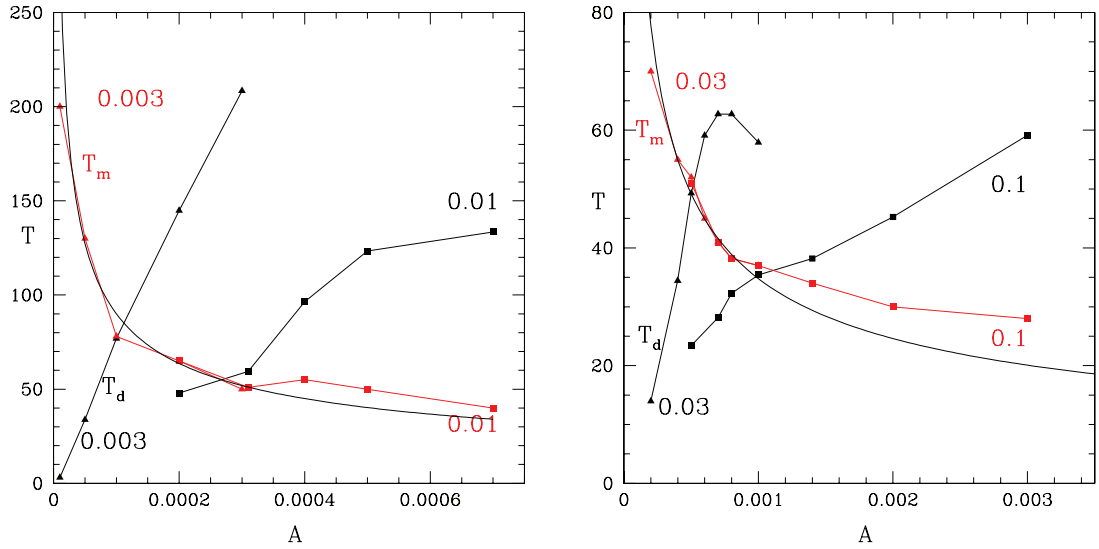

Figure 6. Time for local collisional diffusion across island width, $T_d = w^2/D$, and collisionless mixing time T_m, for $\nu = 0.003\,\nu_0$, $\nu = 0.01\,\nu_0$, (left) and $\nu = 0.03\,\nu_0$, $\nu = 0.1\,\nu_0$ (right). The crossing of the curves for T_d and T_m gives a reasonably accurate determination of the saturation amplitude. The mixing times are fit approximately with $T = c/\sqrt{A}$, as is shown in the smooth black curves with no markings.

collisionality ranged from 0.003 times a characteristic value of $\nu_0 = 1/t_0$ with $t_0 = 30$ ms to 10 times this, giving a range of over three orders of magnitude. The resulting saturation amplitudes ranged from 10^{-4} to 6×10^{-3}, almost two orders of magnitude. The largest collisionality value, $\nu = 10\nu_0$ is seen to result in a saturation level approximately equal to the next smaller value, $\nu = 3\nu_0$, indicating that the collision rate has exceeded the resonance mixing time, not allowing particles to transfer energy and momentum to the mode before scattering out of resonance. For very low collisionality the saturation is less well determined, as there are large oscillations in the final mode amplitude.

There are several pieces of data useful for checking theoretical predictions for mode saturation amplitude. They include, beside mode amplitude and collision frequency, the inital linear growth rate and damping, the bounce or mixing time within a resonance island at saturation, the island width, or in cases of large amplitude, the extent of the stochastic domain, and the local collisional diffusion rate due to the mode.

The domain of broken KAM surfaces [25] is determined by the method of phase vector rotation [14]. This method is used to determine the significant resonances. The island width for significant resonances is further envisioned using a Poincaré plot. In figure 4 is shown the P_ζ, E plane with the dominant resonance seen to be at $P_\zeta/\psi_w = -0.1$ for a particle energy of 55 keV. There are of course no collisions present for the construction of this plot. The resonance is in the domain of co-passing orbits, labelled P, bounded on the right by the magnetic axis, on the left by the plasma edge, and on the bottom by the triangular domain of trapped orbits, labelled T. The canonical momentum P_ζ is normalized to the value of poloidal flux at the plasma edge, ψ_w. This Poincaré plot is also made for $\mu B = 20$ keV, along the path shown in blue in the P_ζ, E plane, where the distribution is strongly peaked, and for the particle energy of 55 keV. There are of course resonances at all values of μ and particular values of P_ζ and E in the distribution. Nevertheless an examination of the single strong resonance seen in figure 4 is sufficient to discover the saturation amplitude and mechanism.

The resonant island can be shown in the variables E,θ or ψ_p,θ, or P_ζ,θ. Poloidal flux as a choice is not useful, because even without a perturbation due to a mode, this quantity varies strongly in an orbit due to drift motion. It is convenient to choose a variable that is conserved in the absense of perturbations, and we have chosen the canonical momentum P_ζ.

4. A rapid means of determining mode saturation

In this section we introduce a means of determining single mode saturation amplitude without going through a lengthy simulation of mode growth. The method hinges on the simple recognition that particles within the resonance give their energy to the mode on the time scale of the particle bounce frequency. Since the bounce frequency is a function of distance from the resonance O-point, the resulting motion produces a mixing of different particle energies resulting in a partial flattening of the distribution. This is a collisionless process. On the other hand new particles are diffusing into the resonance from the nearby distribution at the local collisional diffusion rate, attempting to reestablish the density gradient. Thus one can hypothesize that mode saturation occurs when the resonance island has grown to the point where these two rates are balanced. But these two rates can be quickly numerically determined for a given mode amplitude, giving a means of finding the saturation amplitude without a lengthy simulation.

In figure 5 is shown a determination of the local collisional diffusion rate, the local collisionless mixing time, and the approximate extent of the domain of broken KAM surfaces, for toroidal canonical momentum P_ζ with a mode amplitude of $A = 3 \times 10^{-4}$ using 5000 particles. This is not

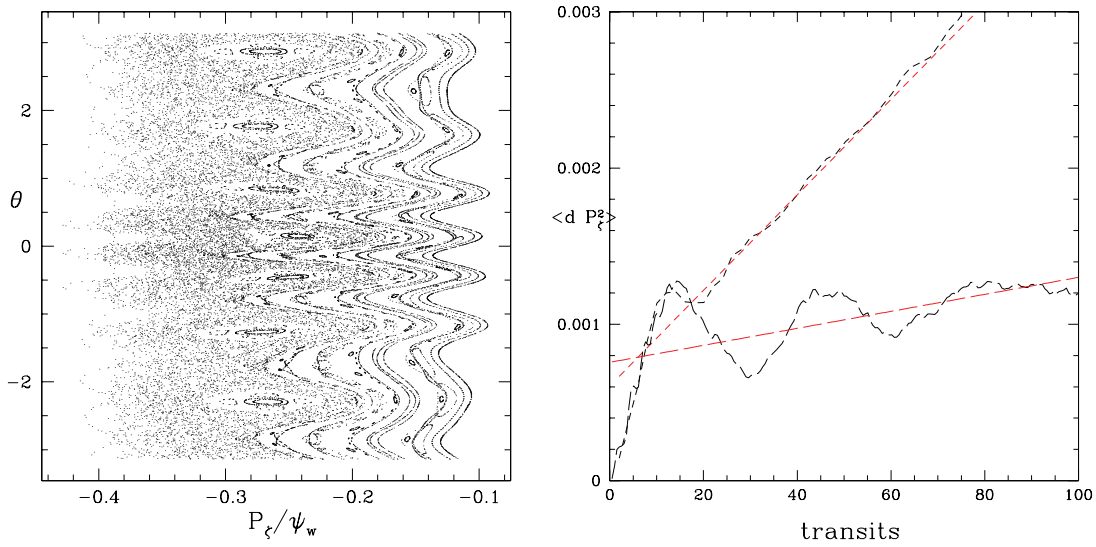

Figure 7. Poincaré plot showing large scale stochasticity (left), and local determination of $\langle dP_\zeta^2 \rangle$ versus time (right), mode amplitude $A = 2.2 \times 10^{-3}$. In the collisionless case (long dashes) the width of the domain of broken KAM surfaces is approximately $W^2 = 10^{-3}$ and the mixing time is about $T_m = 25$, but in fact the last KAM surface has been broken and there is collisionless diffusion leading to loss. The collisional case is shown with short dashes. Shown in red are linear least square fits to the data.

the saturation amplitude for any of the chosen values of collisionality, simply an arbitrary amplitude to demonstrate the method. The plots are obtained by launching particles with values of P_ζ, E, and μB all near the resonance location shown in figure 4, but with a distribution of phase relations with respect to the mode.

The collisional plot gives, with a collisionality of $\nu = 0.003\ \nu_0$, a value of diffusion D, with $\langle dP_\zeta^2 \rangle = Dt$, of $D = 9.8 \times 10^{-8}$, units of normalized canonical momentum to transit time. The brackets $\langle\rangle$ refer to a mean over the whole particle distribution, and the value of D is of course the slope of the large time asymptotic value, fit with the red line. The collisionless plot gives the time evolution of particles in the resonance as the distribution asymptotically approach flattening. There is an initial large change in $\langle P_\zeta^2 \rangle$ as particles on the high energy side of the resonance move to the low side, and vice versa, with a time given by the particle bounce time in the resonance. This can be used as a definition of the mixing time, made precise by using the first crossing of $\langle dP_\zeta^2 \rangle$ with the final saturation value, after the initial overshoot, of $T_m = 50$. The final value of $\langle dP_\zeta^2 \rangle$ gives a determination of the extent of the broken KAM surfaces, given by its asymptotic value, seen to be $W^2 = 2 \times 10^{-5}$. Here island width W is given in terms of canonical momentum. The time for particles to diffuse across W is then given by $T_d = W^2/D$. Times are given in toroidal transit times and distances in the space of canonical momentum.

In figure 6 are shown the values of the collisional diffusion time T_d and the mixing time T_m as a function of mode amplitude, for collision rates of $\nu = 0.003\,\nu_0, \nu = 0.01\,\nu_0, \nu = 0.03\ \nu_0$ and $\nu = 0.1\ \nu_0$. In all these cases as the mode amplitude increases the mixing time decreases, indicating a more rapid resonance bounce, and the scaling is given by $T_m = c/\sqrt{A}$, as is shown with the black lines giving an approximate fit for amall amplitude. The collisional diffusion rate D is approximately linear in the mode amplitude, but the width of the domain of broken KAM surfaces is proportional to A^2, as seen in figure 5, so the diffusion time $T_d = W^2/D$ increases with A. The crossing of these two curves gives a determination of the saturation amplitude. These values are seen to cross at the observed saturation amplitude of the mode within numerical error of the determinations, indicating that the balance between collisional diffusion across the domain of broken KAM surfaces and the mixing time within this domain is a good method of determining saturation width. In reference [21] a similar method is elaborated using orbital dynamics within an island, but this kind of analysis depends on detailed information regarding the resonance and is of course not simply applicable when the distribution is not given analytically.

However for larger collisionality the qualitative nature of these plots changes. In figure 7 is a Poincaré plot showing large scale stochasticity, and local determination of $\langle dP_\zeta^2 \rangle$ versus time, with and without collisions, with mode amplitude $A = 2.2 \times 10^{-3}$. In the collisionless case the width of the domain of broken KAM surfaces is approximately $W^2 = 10^{-3}$ and the mixing time is about $T_m = 25$, but in fact the collisionless value does not asymptote to a constant, it is unbounded, the last KAM surface has been broken and there is collisionless diffusion leading to loss. Shown in red are linear least square fits to the data. In figure 8 are shown the values of the collisional diffusion time T_d and the mixing time T_m as a function of mode amplitude, for collision rates of $\nu = 0.3\ \nu_0$, $\nu = \nu_0$, $\nu = 3\ \nu_0$ and $\nu = 10\ \nu_0$. In all these cases the mixing time T_m is taken to be the value of the first crossing shown in figure 5, which is an arbitrary but precise determination of the internal equilibration time. For values of $\nu = \nu_0$ and

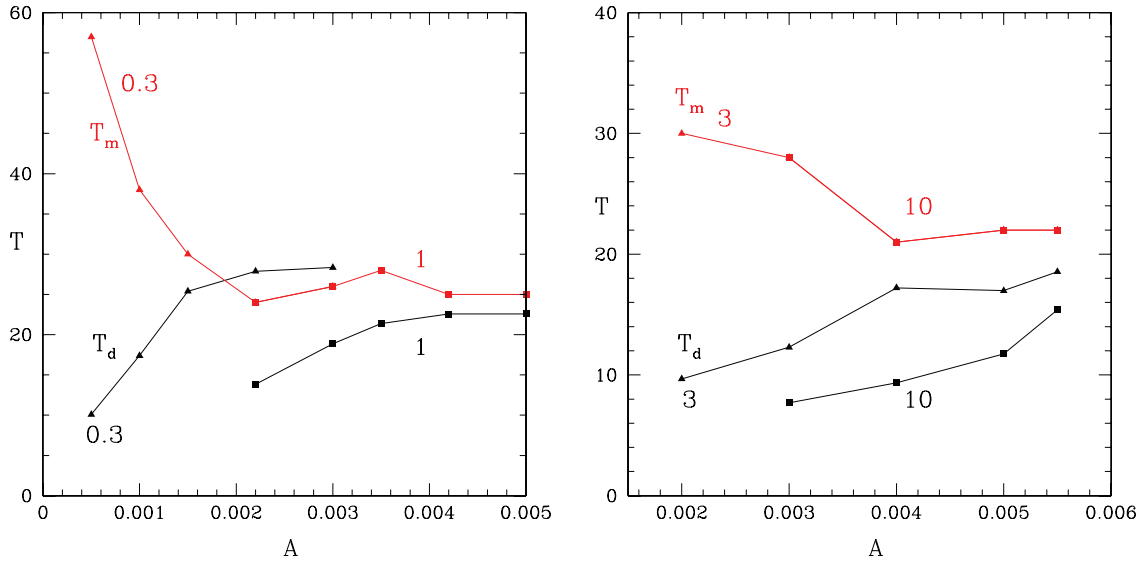

Figure 8. Time for local collisional diffusion across island width, $T_d = w^2/D$, and collisionless mixing time T_m, for $\nu = 0.3\,\nu_0$, $\nu = \nu_0$ (left), and $\nu = 3\nu_0$, $\nu = 10\nu_0$ (right). The collisionless mixing time values are of course independent of the collision value, the curves are labelled merely to denote the domain of amplitude range for comparison with the collisional values. For all values of collisionality equal or larger than $\nu = \nu_0$ there is no steady state, the plots of T_m and T_d do not cross.

Table 1. Mode saturation data.

ν	ν s^{-1}	A	w^2	T_m	D	T_d	k
0.003	0.10	0.000 13	2.716×10^{-6}	78	3.53×10^{-8}	77	6.3×10^{-3}
0.01	0.33	0.000 31	2.19×10^{-5}	49	2.97×10^{-7}	59	6.6×10^{-3}
0.03	1.00	0.0006	1.02×10^{-4}	45	1.9×10^{-6}	52	6.0×10^{-3}
0.1	3.33	0.0014	3.25×10^{-4}	34	8.51×10^{-6}	38	6.5×10^{-3}
0.3	10.0	0.0022	1×10^{-3}	25	2.87×10^{-5}	27.8	4.9×10^{-3}
1	33.3	0.0042	2.2×10^{-3}	22	9.75×10^{-5}	22.5	4.2×10^{-3}
3	100	0.0055	4.3×10^{-3}	22	1.78×10^{-4}	18.5	2.6×10^{-3}
10	333	0.0055	$4. \times 10^{-3}$	22	$2.6 \times 10^{-4}4$	15.4	1.2×10^{-3}

larger there is no interception of T_d and T_m, also indicating that no saturation occurs. This is the case for all higher values of collisionality. Clearly the destruction of bounding KAM surfaces, allowing particles to leave the resonance domain, decreases the mixing rate, and T_m increases or remains constant with increasing mode amplitude, instead of decreasing as in figure 6.

In table 1 is given the saturation data, including the collision frequency, the saturation amplitude in units of major radius, the width W of the domain of broken KAM surfaces squared, with width in units of canonical momentum P_ζ/ψ_w, the local mixing time T_m as given by the second crossing of the collisionless time history with the final steady state width, the local collisional diffusion rate D, and the derived time for diffusion across the width of the domain, $T_d = w^2/D$. The times are given in units of the transit time. Also shown is the constant k relating the amplitude A to the collisionality through equation (11). It is seen that this number is reasonably constant for amplitudes for which the resonance is well defined, but begins to fail as the stochastic domain is approached.

Some work has been done on determining mode saturation [7–9, 19]. In particular, a simple model gives for saturation [8]

$$\omega_b = \frac{\nu_{\rm eff}\gamma_L}{\gamma_d} \tag{10}$$

where $\nu_{\rm eff} = \nu_d(\omega/\omega_b)^2$ and ω_b is the bounce frequency in the resonance, γ_L the linear growth rate, ν_d the pitch angle scattering frequency, and γ_d the damping due to background dissipation. Substituting the fact that $\omega_b = 2\pi/T_m$ is proportional to $\sqrt{A}$, upon writing $\omega_b/\omega = (A/A_0)^{1/2}$ we find

$$A = A_0(\nu/\omega)^{2/3}(\gamma_L/\gamma_d)^{2/3} = k\nu_d^{2/3} \tag{11}$$

where for all the simulations in this paper, A_0 and k are constants. Other important parameters are the mode frequency, $\omega = 111$ kHz, the damping $\gamma_d/\omega = 0.0014$, and the linear growth rate $\gamma/\omega = 0.028$. Inserting $\gamma_L/\gamma_d = 20$ and for $\nu = 0.01\nu_0 = 11$ s^{-1} we find $A_0 = 0.067$. Similarly substituting the value for the mixing time for this value of ν and writing $\omega_b = 2\pi C/T_m$ we find $C = 1.2$, i.e. the mixing time

numerically observed very accurately gives the resonance bounce frequency.

5. Conclusion

The saturation of a toroidal Alfvén mode is studied using the numerical beam particle distribution given by TRANSP, as a function of the pitch angle scattering rate, and is found to scale with the predicted $\nu^{2/3}$ dependence. The major mode-particle resonance is found, and local collisional and collisionless transport properties near this resonance give a novel means of determining saturation levels. Although this work considers a single mode, and the situation in a typical discharge includes many modes, the single mode saturation values can probably serve as good intial values for a multi mode simulation, with subsequent mode amplitude modification through the change of the particle distribution perturbing these values. This will be investigated in future work. Multi mode simulations also require a multi-processor extension of the present code.

Acknowledgment

This work was partially supported by the U.S. Department of Energy Grant DE-AC02-09CH11466. Muni Zhou acknowledges support of Zhejiang University for a visit to PPPL. The digital data for this paper can be found in http://arks.princeton.edu/ark:/88435/dsp018p58pg29j.

References

[1] ITER Physics Basis Editors and ITER Central Team 1999 *Nucl. Fusion* **39** 122138
[2] Heidbrink W W 2008 *Phys. Plasmas* **15** 055501
[3] White R B, Gorelenkov N N, Heidbrink W W and Van Zeeland M A 2010 *Phys. Plasmas* **17** 056107
[4] White R B, Gorelenkov N N, Heidbrink W W and Van Zeeland M A 2010 *Plasmas Phys. Control. Fusion* **52** 045012
[5] Van Zeeland M A *et al* and ASDEX Upgrade Teams 2011 *Phys. Plasmas* **18** 056114
[6] Collins C S, Heidbrink W W, Austin M E, Kramer G E, Pace D C, Petty C C, Stagner L, Van Zeeland M A, White R B and Zhu Y B 2016 *Phys. Rev. Lett.* **116** 095001
[7] Berk H L and Breizman B N 1990 *Phys. Fluids* B **2** 2226
Berk H L and Breizman B N 1990 *Phys. Fluids* B **2** 2235
Berk H L and Breizman B N 1990 *Phys. Fluids* B **2** 2246
[8] Berk H L, Breizman B N and Huanchun Ye 1992 *Phys. Rev. Lett.* **68** 3563
[9] Berk H L, Breizman B N and Pekker M 1996 *Phys. Rev. Lett.* **76** 1256
[10] Lilley M K, Breizman B N and Sharapov S E 2010 *Phys. Plasmas* **17** 092305
[11] Kaye S M *et al* 2005 *Nucl. Fusion* **45** S168–80
[12] White R B, Gorelenkov N, Gorelenkova M, Podesta M, Ethier S and Chen Y 2016 *Plasma Phys. Control. Fusion* **58** 115007
[13] White R B 2014 *The Theory of Toroidally Confined Plasmas* 3rd edn (London: Imperial College Press)
[14] White R B 2012 *Commun. Nonlinear Sci. Numer. Simul.* **17** 2200
[15] White R B 2011 *Plasma Phys. Control. Fusion* **53** 085018
[16] White R B 2015 *Plasma Phys. Control. Fusion* **57** 115008
[17] Boozer A H and Kuo-Petravic G 1981 *Phys. Fluids* **24** 851
[18] Chen Y, White R B, Fu G-Y and Nazikian R 1999 *Phys. Plasmas* **6** 226
[19] Gorelenkov N N, Chen Y, White R B and Berk H L 1999 *Phys. Plasmas* **6** 629
[20] Lang J, Fu G-Y and Chen Y 2010 *Phys. Plasmas* **17** 042309
[21] Wang X, Briguglio S, Lauber Ph, Fusco V and Zonca F 2016 *Phys. Plasmas* **23** 012514
[22] Pankin A, McCune D, Andre R, Bateman G and Kritz A 2004 *Comput. Phys. Commun.* **159** 157
Pankin A, McCune D, Andre R, Bateman G and Kritz A 2009 *Phys. Plasmas* **16** 122505
[23] Gorelenkov N N, Cheng C Z and Fu G 1999 *Phys. Plasmas* **6** 2802
[24] Cheng C Z 1992 *Phys. Rep.* **211** 1–51
[25] Kolmogorov A N 1957 *Proc. Int. Congr. Mathematicians (Amsterdam) vol* 1 p 315
Arnold V I 1963 *Russ. Math. Surv.* **18** 9
Moser J 1962 *Math. Phys. Kl.* II **1** 1